Published in Physical Review A 71: 022712, 2005

Elastic scattering, vibrational excitation, and attachment in low-energy electron-SF_6 scattering: Experiment and effective range theory

Ilya I. Fabrikant
Department of Physics and Astronomy, University of Nebraska, Lincoln, Nebraska 68588-0111, USA

Hartmut Hotop
Fachbereich Physik, Technische Universität, 67653 Kaiserslautern, Germany

Michael Allan
Département de Chimie, Université de Fribourg, 1700 Fribourg, Switzerland

Cross sections at low energies for vibrationally elastic and inelastic scattering, as well as electron attachment to SF_6, have been calculated using a multichannel effective range theory (ERT) with complex boundary conditions. The most active vibrational modes, the totally symmetric mode ν_1 and the infrared active mode ν_3, have been included in the calculation. The ERT parameters were fitted to reproduce the experimental total and attachment cross sections. Differential elastic and vibrational excitation cross sections have been measured at 30° and 135° using a spectrometer with hemispherical analyzers. The calculation reproduces correctly the magnitudes and shapes of the differential elastic and ν_1, ν_3, and $2\nu_1$ excitation cross sections, in particular the sharp structures at vibrational thresholds. The *s*- and *p*-wave phase shifts obtained in the present analysis differ from those recently derived by Field *et al.*

DOI: 10.1103/PhysRevA.71.022712 PACS number(s): 34.80.Gs

I. INTRODUCTION

Sulfur hexafluoride is commonly used as a gaseous dielectric and as a plasma etching gas [1]. It is an efficient absorber of infrared radiation, and at the same time very stable. As a result, it has a high global warming potential and is of environmental concern [1]. At the same time the physics of low-energy e-SF_6 scattering is very interesting [2]. First, SF_6 has a high electron elastic scattering cross section [1,3,4] and a large rate for electron attachment at very low energies [1,2]. An *ab initio* theoretical description of these results is very challenging. First calculations [5] of elastic e-SF_6 collisions show a sharp increase of the a_{1g} cross section near zero energy, although the authors emphasize that this result should be considered as tentative because "we normally do not attach too much credence to the results of the present model below a couple of tenths of eV." Moreover, recent calculations [6] of elastic cross sections fail to reproduce the high values measured at low energies [3,4].

Second, low-energy electron attachment to SF_6 leads to the formation of metastable anions SF_6^- [1,2] whose lifetime is of the order of a few ms [7]. The nondissociative attachment process for SF_6 is described quite well by the Vogt-Wannier model [8] for electron capture into the polarization well and by its simplified version [9]. However, the Vogt-Wannier model is phenomenological in the sense that it does not incorporate the actual physical mechanism for electron trapping. In fact the long lifetime of SF_6^- is explained by intramolecular vibrational energy redistribution (IVR) [10,11]. According to this scenario [10], at the first stage the incoming *s*-wave electron distorts the nuclear framework by coupling to the symmetric stretch motion with simultaneous capture. The symmetric ν_1-mode in SF_6 is strongly Raman active [12] and therefore intensively interacts with the spherically symmetric charge distribution due to the *s*-wave electron. The energy deposited by the electron is then distributed over all the nuclei in a chaotic long-lived anion state before the nuclear framework can oscillate back to its initial configuration. This process is very well studied in molecular spectroscopy [13], but has not received as much attention in the field of electron-molecule collisions. Although the potential energy curve of SF_6^- in the octahedrally symmetric configuration has been studied by several authors [14], there are no studies of the multidimensional potential surfaces necessary for IVR calculations.

The low-energy behavior of e-SF_6 scattering is connected to the near-threshold behavior of vibrational excitation. The threshold peak observed by Rohr [15,16] in vibrational excitation of the ν_1 mode was the first example of a nonpolar molecule exhibiting such a behavior.

In the present paper we use a semiempirical approach to IVR by combining the effective range theory (ERT) with complex boundary conditions to describe elastic scattering, attachment, and vibrational excitation of the symmetric stretch mode ν_1 and infrared active mode ν_3. The results are compared with attachment cross sections measured with the laser photoelectron attachment (LPA) method, with differential elastic and vibrational excitation cross sections measured in a crossed-beam experiment, and with the total and backward cross section of Field *et al.* [4].

II. THEORETICAL METHODS

A. Effective range theory with complex boundary conditions

Effective range theory (ERT) is a limiting case of the *R*-matrix theory, therefore we will start with the basic equa-

tions of the latter [17–19]. We divide the whole space into two regions separated by a sphere of radius r_0. Assuming first octahedral geometry, we approximate the electron-SF_6 interaction outside the sphere by the isotropic polarization potential $-\alpha/2r^4$ independent of the nuclear geometry. This approach replaces the octahedrally symmetric e-SF_6 interaction by a spherically symmetric interaction and replaces the polarization coupling leading to the Raman activity of the symmetric stretch ν_1 mode by a short-range coupling inside the sphere (see below). For low-energy scattering dominated by s and p waves these approximations are justified. Corrections due to deviations from octahedral geometry will be discussed in the next section.

The solution ψ of the corresponding radial Schrödinger equation is matched with the internal wave function in the fixed-nuclei approximation in the form

$$\psi(r_0,q) = R(q) \left. \frac{d\psi(r,q)}{dr} \right|_{r=r_0}, \tag{1}$$

where r stands for the electron radial coordinate, and q for the set of all internuclear coordinates. To obtain the R matrix with the account of nuclear dynamics, we use the Born-Oppenheimer approximation [17]. First we write the fixed nuclei R matrix in the form

$$R(q) = \sum_{\lambda=0}^{\infty} \frac{\gamma_\lambda^2(q)}{E_\lambda(q) - E_e}, \tag{2}$$

where E_λ and γ_λ are eigenvalues and surface amplitudes for the fixed-nuclei problem, and E_e is the electron energy. We are mostly interested in s-wave scattering when the poles $E_\lambda(q)$ do not represent resonance states. However, the lowest pole ($\lambda=0$) represents a bound state in the range of q where the negative ion is stable.

We will assume now that the q-dependence and the energy dependence of all terms in sum (2) except the first is weak so that $R(q)$ can be rewritten in the form

$$R(q) = \frac{\gamma_0^2(q)}{E_0(q) - E_e} + R_b, \tag{3}$$

where the background term R_b is independent of q and E_e. This is the usual assumption of the resonance R-matrix theory [18,19]. It is justified in our case as well because the interaction between the electron motion and the nuclear motion is weak in electronically excited states ($\lambda>0$), and the electron energy E_e is small compared to the potential energy of interaction between the electron and the molecule.

We now include nuclear motion by adding the kinetic energy operator in the denominator of the R matrix. As a result, R becomes an integral operator

$$R(q) = \gamma_0(q)(H_I - E)^{-1}\gamma_0(q) + R_b, \tag{4}$$

where E is the total energy of the system, $H_I = T(q) + U(q)$, and $U(q) = E_0(q) + V(q)$, where T is the kinetic energy operator for the nuclear motion, $V(q)$ is the potential energy surface for the neutral molecule. In the presence of a dissociative attachment channel we modify the R operator by the replacement $E \to E + i0$. This corresponds to outgoing-wave boundary conditions when one of the internuclear coordinates goes to infinity. However, the dissociative attachment channel is practically absent in electron scattering by SF_6 at electron energies below about 0.2 eV for thermal gas temperatures ($T=300$ K) [1,20]. Attachment occurs due to IVR whereby the vibrational energy initially concentrated in the active symmetric mode ν_1 is redistributed among other modes (so-called bath modes) and is thus not available for autodetachment of the electron on the time scale of the experiment. A complete *ab initio* treatment of this process requires calculations of the vibrational dynamics on the multidimensional potential surface $U(q)$. Thoss and Domcke [11] showed that the problem can be simplified in the Markov approximation for the interaction between the active mode and the bath modes by adding an energy independent width and shift to the system Hamiltonian, that is to the part of the Hamiltonian containing the coordinates of only the active mode. Accordingly we will replace the Hamiltonian $H_I(q)$ by $H_I^e(s) = T(s) + U(s) - i\Gamma(s)/2$, where s is the active normal coordinate, in our case it is the symmetric stretch coordinate corresponding to the ν_1 mode. Like in the optical model, H and the R operator become now non-Hermitian, and the attachment cross section is determined from the S-matrix unitarity defect.

The attachment dynamics is controlled by the transition region from the virtual state of SF_6^- into the bound state. This is the region close to the pole of the operator $(H_I^e - E)^{-1}$. Therefore, to develop ERT, we rewrite Eq. (1) in the form

$$\frac{d\psi}{dr} = (R^e)^{-1}(s,E)\psi, \tag{5}$$

with

$$R^e(s,E) = \gamma_0(s)[H_I^e(s) - E]^{-1}\gamma_0(s) + R_b, \tag{6}$$

where all arguments of γ_0 other than s are taken at the equilibrium internuclear separation.

We will return now to the fixed-nuclei approximation at $r<r_0$ and replace the complex operator $(R^e)^{-1}(s,E)$ by a complex function $f(s,E)$. In the spirit of the ERT of Gauyacq and Herzenberg [10,21], we expand $f(s,E)$ in powers of s (assuming that $s=0$ corresponds to equilibrium) and keep only the zero-order and the linear terms

$$f = f_0 + f_1 s, \tag{7}$$

where f_0 and f_1 are complex parameters which generally depend on the electron energy. In the first order approximation of ERT, we neglect this energy dependence and consider f_0 and f_1 as complex constants. We stress that the energy dependence of the cross sections is taken care of by the external wave functions ψ, and this dependence can be very significant at low energies because of the long-range electron-molecule interaction.

Using the harmonic oscillator approximation for the neutral molecule, we obtain the matrix of logarithmic derivatives in the form

$$f_{v'v} = f_0\delta_{vv'} + \frac{f_1}{\sqrt{2\mu\omega}}[\sqrt{v}\,\delta_{v'v-1} + \sqrt{v+1}\,\delta_{v'v+1}],$$

where $\mu = 6M_F$ and ω are the effective mass and frequency for the symmetric stretch vibrations. The matrix of the outside solutions can be written as

$$\psi = \psi^- - \psi^+ S,$$

where $\psi^{\pm}$ are matrices of the outgoing and ingoing solutions and S is the scattering matrix. The matching equation is solved for S from which we obtain elastic, vibrational excitation and reaction cross sections. The complex parameters f_0, f_1 are fitted to reproduce experimental data for attachment (Klar *et al.* [20]) and total (Field *et al.* [4]) cross sections at several energy points within the interval between 0.01 and 0.18 eV. The obtained values of the ERT parameters are $f_0 = 0.9894 + 0.1081i$, $f_1 = -15.18 - 3.41i$. These values lead to a slight violation of the conservation of probability above $E = 0.22$ eV. It appears as a negative attachment cross section which reaches -4.5 Å^2 at $E = 0.4$ eV. It is still small, though, compared to the total cross section at this energy, $\sigma_t = 49.3$ Å^2. We therefore expect the present ERT parameters to give reasonable results for energies up to 0.4 eV. At higher energies the energy dependence of f should be incorporated.

B. Inclusion of the infrared active mode

Excitation of the infrared active mode ν_3, associated with vertical displacement of the apical F atoms, is substantial at low electron energies. Although a significant part of it is due to the direct process caused by the transition dipole moment, it is important to investigate the contribution due to the negative-ion state. Highly resolved experimental attachment cross sections [20,22] show significant structure at the ν_3 excitation threshold indicating the coupling of the ν_3 channel with other channels.

To incorporate this effect in the ERT theory, we include the dipolar interaction which couples the ν_3 channels in the outer region. This coupling involves higher electron angular momenta. In the inner region we assume that the electron wave function in channels with higher angular momenta is affected only by the centrifugal barrier, and calculate the logarithmic derivative at the R-matrix surface as $f_{ll'} = (l+1)/r_0\delta_{ll'}$ for either l or l' exceeding 0.

The negative-ion state contribution to the excitation of the ν_3 mode is most important for the $l = 1 \rightarrow 0$ transitions. Since the centrifugal barrier becomes high at $l \geqslant 2$ and low energies considered by us, we include only s and p wave contributions in the ERT calculations. Moreover, since we are mostly interested in the influence of the $\nu_3 = 1$, $l = 0$ channel on the elastic and attachment cross sections dominated by the s-wave, we proceed with the following approximate treatment of the $l = 1$ channels.

Consider e-SF_6 scattering in the body frame with the z axis oriented along one of the symmetry axis of SF_6. If initially $l = 0$, excitation of all 3 degenerate ν_3 modes (along x, y, and z axis) occurs with the same amplitude. In the final channels we have $l = 1$, $m = 0$ for the z-excitation, and $m = \pm 1$ for x and y excitation. All these channels can be considered as weak. Accordingly, we include coupling only with $m = 0$. The solution of the coupled equations gives the cross section for excitation of vibrations along z axis, therefore we multiply this result by 3. (A similar treatment was used by Takekawa and Itikawa in their studies of excitation of degenerate bending vibrations in CO_2 [23].) If initially $l = 1$ and $m = 0$, only z-excitation is possible, since we neglect $l \geqslant 2$. If initially $l = 1$, $m = \pm 1$, we obtain exactly the same set of coupled equations for x and y excitations, therefore this case does not require a separate treatment.

For higher partial waves the Born dipole approximation is adequate. For the total vibrational excitation cross section $v = 0 \rightarrow v' = 1$ we use the standard closure formula (see, e.g., Ref. [24]):

$$\sigma_{vv'} = \frac{8\pi}{3k_v^2}D_{vv'}^2\left[\ln\frac{k_v + k_{v'}}{k_v - k_v'} - 2k_v k_v'(R_{01}^2 + R_{10}^2)\right] + \frac{\pi}{k_v^2}(|S_{01}|^2 + |S_{10}|^2), \tag{8}$$

where k_v and $k_{v'}$ are initial and final electron momenta, $D_{vv'}$ the transition dipole moment, $S_{ll'}$ the scattering matrix elements obtained from the solution of the close-coupling equations, and

$$R_{ll'} = \int j_l(k_v r) j_{l'}(k_{v'} r)\,dr, \tag{9}$$

where $j_l(x)$ is the spherical Bessel function. The radial matrix elements entering Eq. (8) can be expressed as [25]

$$R_{01} = \frac{1}{4k_v x}\left(2 - \frac{1-x^2}{x}\ln\frac{1+x}{1-x}\right),$$

$$R_{10} = \frac{1}{4k_v}\left(2 + \frac{1-x^2}{x}\ln\frac{1+x}{1-x}\right), \tag{10}$$

where $x = k_{v'}/k_v$.

For the calculation of the differential cross section, it is more efficient to use closure for the amplitudes for excitation of rotational substates $f_{j\mu}(\theta,\phi)$ in the sudden approximation with respect to rotations [26]:

$$f_{10}(\theta) = \frac{2i}{\sqrt{3}}D_{vv'}\left(\frac{k_{v'}\cos\theta - k_v}{q^2} + R_{10} - R_{01}\cos\theta\right) + \frac{1}{2\sqrt{k_v k_{v'}}}(S_{10} - S_{01}\cos\theta), \tag{11}$$

$$f_{11}(\theta,\phi) = \left[i\sqrt{\frac{2}{3}}D_{vv'}\left(R_{01} - \frac{k_{v'}}{q^2}\right) + \frac{1}{2\sqrt{2k_v k_{v'}}}S_{01}\right]\sin\theta e^{-i\phi}, \tag{12}$$

where $q^2 = k_v^2 + k_{v'}^2 - 2k_v k_{v'}\cos\theta$. The differential cross section is obtained from here as

$$\sigma_{vv'} = \frac{k_{v'}}{k_v}(|f_{10}|^2 + 2|f_{11}|^2), \tag{13}$$

where j, μ are the rotational angular momentum and its projection on a fixed axis. Although these equations were originally written for a diatomic molecule case, they are applicable to a symmetric top as well, if we are not interested in partial cross sections for excitation of $j\mu K$ substates, where K is the projection of the angular momentum j on the molecular axis.

C. Polarizability and transition dipole moment

According to measurements of Kim *et al.* [27], the transition dipole moment for the ν_3 fundamental, D_{01}^z is 0.172 a.u. After accounting for the triple degeneracy of the ν_3 mode, this gives a big contribution, 13.8 a.u., to the polarizability of SF_6. The total vibrational polarizability of SF_6 is 15.2 a.u. [28], the 1.4 contribution being due to the weaker ν_4 mode. The total polarizability of SF_6 is 44.1 a.u. [29] which is consistent with the result for the electronic part of the polarizability, 31.3 a.u., obtained from measurements of the refractive index [30]. Since only one ν_3 mode is included in the close-coupling calculations, we have chosen the effective polarizability 44.1−4.6=39.5 a.u. This approach should be adequate for electron energies well below the ν_3 excitation threshold, the region we are mostly interested in, but it might lead to some inaccuracy above the threshold.

D. Higher partial waves for elastic scattering

To describe elastic scattering in higher partial waves, we use the modified effective range theory of O'Malley *et al.* [31]. For $l \geqslant 2$ the scattering phase shift δ_l at low energies $E = k^2/2$ is

$$\tan \delta_l = \frac{\pi\alpha k^2}{(2l-1)(2l+1)(2l+3)}. \tag{14}$$

Since at low energies δ_l is small for $l \geqslant 1$, we can write for the scattering amplitude $F(\theta)$

$$F(\theta) = F_0 + 3F_1 \cos\theta + \sum_{l=2}^{\infty} \frac{e^{2i\delta_l} - 1}{2ik}(2l+1)P_l(\cos\theta) \tag{15}$$

$$= F_0 + 3F_1 \cos\theta + \pi\alpha k \sum_{l=2}^{\infty} \frac{P_l(\cos\theta)}{(2l-1)(2l+3)}, \tag{16}$$

where F_0 and F_1 are the s-wave and p-wave scattering amplitudes. Finally we obtain [32]

$$F(\theta) = G_0 - B \sin\frac{\theta}{2} + C\cos\theta, \tag{17}$$

where

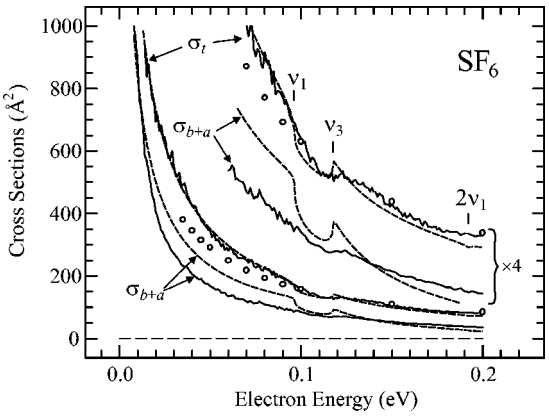

FIG. 1. The total integral cross section σ_t and the sum of the backward scattering and the attachment cross sections, σ_{b+a} (see text). The present theoretical results are shown as dashed lines; the experimental data of Field *et al.* [4] are shown as solid lines. Circles indicate the total integral data of Ferch *et al.* [3], as tabulated by Christophorou and Olthoff [1].

$$G_0 = F_0 + \frac{\pi\alpha k}{3}, \quad B = \frac{\pi\alpha k}{2}, \quad C = 3F_1 - \frac{\pi\alpha k}{5}.$$

Equation (17) allows us to find the integrated elastic cross section $\sigma_{\rm el}$ and the cross section for elastic scattering into the back hemisphere $\sigma_{b,\rm el}$

$$\sigma_{\rm el} = 2\pi\left(2|G_0|^2 - \frac{8}{3}B\,\mathrm{Re}\,G_0 + B^2 + \frac{2}{3}|C|^2 + \frac{8}{15}B\,\mathrm{Re}\,C\right), \tag{18}$$

$$\sigma_{b,\rm el} = 2\pi\left[|G_0|^2 - \frac{2}{3}(4-\sqrt{2})B\,\mathrm{Re}\,G_0 + \frac{3}{4}B^2 + \frac{1}{3}|C|^2 + \frac{4}{15}(2+\sqrt{2})B\,\mathrm{Re}\,C - \mathrm{Re}(G_0C^*)\right]. \tag{19}$$

The latter is necessary for comparison with the measurements of Field *et al.* [4], who, in addition to the total cross section, have measured the sum of σ_b and the attachment cross section.

III. EXPERIMENTAL METHODS

A. Origin of angle-integrated scattering and attachment cross sections

In the present work, the parameters of the ERT theory are fixed with reference to presently available absolute cross sections for (i) total electron scattering (labeled σ_t) and (ii) electron attachment (labeled σ_a) involving a static SF_6 target at the gas temperature $T_G = 300$ K (Figs. 1 and 2). The cross sections for total electron scattering are taken from the recent work of Field *et al.* [4] which extend down to energies around $E = 0.01$ eV; for comparison we also show the earlier results of Ferch *et al.* [3] ($E \geqslant 0.035$ eV). Field *et al.* [4] use a linear electron transmission technique with the option of a superimposed axial magnetic guiding field. The electrons are

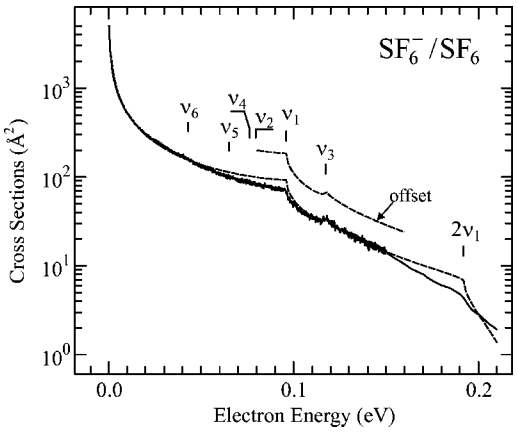

FIG. 2. The attachment cross section σ_a from the LPA experiment (solid) and the present ERT calculation (dashed). Part of the theoretical curve is shown vertically offset for clarity.

produced by photoionization of ground state argon atoms close to threshold at photon bandwidths of 1–2 meV [33], extracted by a nearly homogeneous electric field (which does not lead to significant further energy broadening because of the tight focus of the monochromatized synchrotron radiation), and imaged into the scattering cell by a lens system [33]. Without magnetic field ($B=0$), the experiment yields the sum cross section for all processes which lead to electron loss from the beam transmitted through the scattering chamber [4]. These processes include elastic scattering (except for a very narrow angular range around the forward direction; cross section denoted $\sigma_{\rm el}$), attachment, and vibrationally inelastic processes ($\sigma_{\rm inel}$), i.e.,

$$\sigma_t = \sigma_{\rm el} + \sigma_a + \sigma_{\rm inel}. \tag{20}$$

Within the experimental uncertainties the latter process is only relevant for collision energies above the onset for excitation of the symmetric stretch ($\nu_1=1$, $E=0.096$ eV), as will become clear from the energy loss spectra reported below. In the presence of a magnetic field ($B\approx 0.002$ T), the transmission experiment measures a quantity which is termed backward and attachment cross section and denoted σ_{b+a}. This cross section includes attachment and all elastic and inelastic scattering events which lead to electrons scattered into the backward hemisphere (90°–180°) and are subsequently lost [4]. Thus

$$\sigma_{b+a} = \sigma_{b,\rm el} + \sigma_{b,\rm inel} + \sigma_a. \tag{21}$$

The measurement of σ_{b+a} depends sensitively on the capacity of the instrument to remove all backward scattered electrons and preventing that they return into the forward direction by reflection from the potential barrier which serves to accelerate the primary near-threshold electrons. Thus, part of the backscattered electrons would be registered as unscattered electron flux. Field *et al.* argue that complete loss of the backscattered electrons is provided by trochoidal side motion of the electrons in the lens system due to the action of *transverse* electric fields in combination with the axial guiding magnetic field and subsequent loss at the walls of collimating apertures [4].

The attachment cross section (also used for fixing the theoretical parameters) is due to the combined laser photoelectron data of Klar *et al.* [20] and Hotop *et al.* [34] for a static SF_6 gas at $T_G=300$ K. Building on earlier photoelectron attachment work [35], Klar *et al.* [20] used resonant two-photon ionization of metastable $Ar^*(4s\ ^3P_2)$ atoms to create energy-variable electrons over the range 0–173 meV at photon energy widths of 150 μeV or 50 μeV (and in one case below 1 μeV when a single mode dye laser was used for the photoionizing step [36]). The overall energy width of this laser photoelectron attachment (LPA) experiment is limited by the Doppler effect (present in both the photoelectron production and the electron attachment process) and by residual electric fields. For the data taken with the static SF_6 gas an overall energy width around 0.2 meV was achieved at energies below about 3 meV [20,34]. We note that recent work involving supersonic beams of SF_6 seeded in Xe [22] or He [37] essentially confirmed the results of Klar *et al.* [20], but additional structure (e.g., at energies around $E=45$ meV) became apparent, possibly due to the fact that the molecules in the seeded supersonic beam have undergone some vibrational cooling. Since the scattering experiments refer to SF_6 gas at temperatures close to 300 K, the supersonic beam experiments are not considered further in the present context.

An important aspect in the determination of the absolute size of the attachment cross section is the fact that the LPA experiment itself yields only relative energy dependent electron attachment yields $Y_a(E)$ which is proportional to the absolute cross section $\sigma_a(E)=NY_a(E)$ for anion formation due to free electron attachment. The absolute scale is established with reference to electron attachment rate coefficients $k_a(E)$, as determined by means of electron swarm experiments, carried out with a Maxwellian electron energy distribution at equal electron and gas temperature $T=T_e=T_G=300$ K [20,35]:

$$k_a(T) = N(2/m_e)^{1/2}\int_0^\infty Y_a(E)E^{1/2}f(E;T)dE \tag{22}$$

with the Maxwellian distribution function

$$f(E;T) = (4/\pi)^{1/2}(k_BT)^{-3/2}E^{1/2}\exp[-E/(k_BT)],$$

where $k_BT=25.85$ meV for $T=300$ K and $\int_0^\infty f(E;T)dE=1$. As shown by Klar *et al.* for the cases of SF_6 [20] and CCl_4 [38], an integration interval (0,170) meV in Eq. (22) is sufficient to guarantee errors below 1% in the normalization. In the evaluation the near-zero energy range requires some care. For SF_6, Klar *et al.* [20] found that an analytical cross section of the form

$$\sigma_a = (\sigma_0/E)[1-\exp(-\beta\sqrt{E})] \tag{23}$$

with $\sigma_0=7130(360)$ Å^2 meV and $\beta=0.405(40)$ meV$^{-1/2}$ represents a very good overall fit to the calibrated absolute LPA cross section over the energy range 0.2 to 90 meV [i.e., the data points deviate by no more than ±5% from the cross section (23)]. This analytical cross section (which is compatible with the Wigner law for *s*-wave attachment) is thus also used to extrapolate to zero electron energy. The uncertainty

of σ_0 mainly reflects the uncertainty in the rate coefficient [39] used in the normalization procedure.

At $T_G = 300$ K attachment to SF_6 is dominated by formation of long-lived SF_6^- anions (the contribution from other anions such as SF_5^- is below 0.1% [20,34,40]). According to Suess *et al.* [7] attachment of near zero energy electrons yields SF_6^- anions with lifetimes around 10 ms, much longer than the SF_6^- detection time in the LPA experiment with pulsed ion extraction which ranged from 40 to 120 μs [40]. Recent LPA experiments with heated seeded supersonic beams [37] indicate that the energy dependence of SF_6^- formation shows a somewhat steeper decline towards higher energies over the range 0–200 meV at higher temperature. This may reflect the fact that towards higher E and T_G the lifetime of the SF_6^- anion drops to values comparable or lower than the mentioned detection times, but quantitative investigations of the lifetime of SF_6^- anions resulting from energy resolved electron attachment over a range of defined gas temperatures have yet to come.

B. Crossed beam electron spectroscopy

The measurements were performed using a spectrometer with hemispherical analyzers [41,42]. The resolution is about 10 meV in the energy-loss mode, that is about 7 meV in the incident electron beam. The beam currents were around 40 pA. The gases were introduced through a single nozzle with a 0.25 mm diameter, made of molybdenum and kept at $\sim$30 °C during the measurements. The energy of the incident beam was calibrated on the 19.365 eV [43] ^2S resonance in helium and is accurate to within ±10 meV. The response function of the spectrometer was determined on the elastic scattering in helium. The correction is only qualitative within the first 100 meV above threshold. The absence of artifact structures in the cross sections was verified by recording elastic and VE cross sections in CO_2.

The absolute values of the elastic cross sections were determined by comparison with the helium elastic cross section of Nesbet [44] using the relative flow method. The principal cause of error are variations of the instrument's sensitivity in the course of the measurements, due to changing chemical condition of the surfaces of the electron optics and collision region surroundings. The problem increases gradually with decreasing electron energy. The magnitude of these drifts leads to an estimate of the confidence limit of the elastic cross sections as ±20% (±40% below 100 meV). The inelastic cross sections were normalized to the elastic cross section and their accuracy is reduced by the uncertainty of the knowledge of the instrument's response function between the elastic and the inelastic peaks to ±30% (±50% within 100 meV above threshold). To test the consistency of the present and published measurements, we also measured the absolute elastic cross sections at 2.7 and 5.0 eV and compare the results with the measurements of Cho *et al.* [45] and of Rohr [16] in Table I. The data of Rohr were taken from Fig. 1 of Ref. [16] and linearly interpolated between 20° and 40°, the linear interpolation being justified by the angular distributions in Fig. 2 of the same reference. The agreement of the present data with that of Rohr is excellent at energies $\geqslant$0.8 eV. The value in parenthesis is not sufficiently reliable for a quantitative comparison but a useful indication that Rohr's and the present data agree qualitatively on the rapid rise of the cross section toward low energies. The data of Cho *et al.* are slightly higher, but the agreement is generally satisfactory.

TABLE I. Comparison of the present differential elastic cross sections (in $Å^2$/sr) with those of Cho *et al.* [45] and Rohr (interpolated between 20° and 40°) [16].

	$\theta = 30°$			$\theta = 135°$	
Energy	Present	Cho *et al.*	Rohr	Present	Cho *et al.*
0.2 eV	5.72			1.97	
0.4 eV	3.06		(2.3)	0.85	
0.8 eV	1.63		1.5	0.58	
2.7 eV	1.95	2.34	1.9	1.21	1.35
5.0 eV	3.48	4.00	3.6	0.75	0.96

IV. RESULTS

A. Angle-integrated elastic scattering and attachment

The results of the fit for the total σ_t and attachment σ_a cross sections are presented in Figs. 1 and 2. The calculated attachment cross section reproduces the cusps at the ν_1 and ν_3 thresholds observed in the attachment experiments [20,22]. However, the ERT attachment cross section is somewhat too high below the ν_1 and $2\nu_1$ thresholds, which perhaps indicates some influence of the other vibrational modes not included in the calculation. Towards higher energies the ERT approximation may be no longer adequate, and the energy dependence of the logarithmic derivative should be included. Another reason for disagreement might be the dependence of the SF_6^- lifetime on energy (an effect not included in the theoretical model): with rising electron energy the lifetime towards autodetachment may decrease (although detailed experiments on this aspect are yet missing; see above) and become shorter than the time for detection of the SF_6^- anions, resulting in an effectively reduced SF_6^- yield.

It is interesting to note that the Vogt-Wannier model [8], whose application to the problem of electron attachment to SF_6 was discussed by us earlier [46], can be considered as a limiting case of ERT when $r_0 \to 0$. This model does not require adjustable parameters because the absorption appears due to the singularity of the $-\alpha/2r^4$ potential, and it works very well below the vibrational excitation threshold. However, in contrast to the multichannel ERT, it is not able to reproduce the threshold cusps.

Using Eq. (19), we have also calculated the sum σ_{b+a} [Eq. (21)] and compared the results with measurements of Field *et al.* [4] in Fig. 1. Between 0.01 and 0.1 eV the measured σ_{b+a} values are about 30% less than calculated. The low measured values imply a very low backward scattering cross section compared to the integral scattering cross section in this energy range, $\sigma_{b,\mathrm{el}}/\sigma_{\mathrm{el}} < 0.2$, as pointed out in Fig. 6 of Ref. [4].

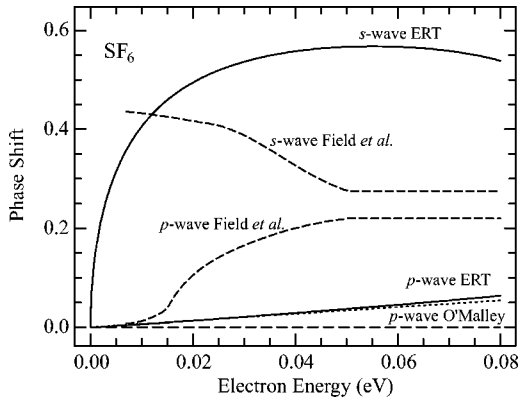

FIG. 3. Phase shifts calculated in this work (solid lines) and derived by Field *et al.* [4]. Dotted line shows the phase shift of O'Malley *et al.* [31].

It is hard to explain the low experimental values of σ_b on theoretical grounds. For example, at $E=0.014$ eV the measured values are (all cross sections are in Å^2) $\sigma_t=936$, $\sigma_{b+a}=585$, $\sigma_a=405$ which means that $\sigma_{\rm el}=531$, $\sigma_{b,\rm el}=180$. The latter value is too small at such a low energy where the scattering should be essentially isotropic, and thus $\sigma_{b,\rm el}$ close to $\sigma_{\rm el}/2$. Our theory yields $\sigma_{b,\rm el}/\sigma_{\rm el}=0.477$ at $E=0.014$ eV. Our attempt to fit the Field *et al.* data for σ_t and σ_{b+a} resulted in an attachment cross section which is too low, and is practically zero above the ν_1 threshold.

This low value of $\sigma_{b,\rm el}$ derived from the measured σ_{b+a} might explain the unexpectedly high values of the *p*-wave scattering phase shifts obtained by Field *et al.* [4] which exceed substantially the MERT values from Eq. (14) and from our calculations. This is demonstrated in Fig. 3, where we present the *s*-wave and *p*-wave scattering phase shifts at energies below the $\nu_1=1$ threshold. Our results for the *s*-wave phase shift are consistent with the main feature obtained by Field *et al.*: the *s*-wave phase shift is positive and quite large at low energies which is due to virtual state scattering. However a strong disagreement is observed in the overall energy dependent behavior.

To obtain the zero-energy cross section, we write the matrix element S_{00}, using the notations of Ziesel *et al.* [47], as

$$S_{00}=\epsilon_0\exp(2i\delta_0).$$

At low energies

$$\delta_0=-Ak,\quad \epsilon_0=1+2Ck,$$

where the parameters A and C can be called real and imaginary parts of the scattering length. Extrapolation of our *S*-matrix down to zero energy gives $A=-18.80$ a.u., $C=-7.35$ a.u., and $\sigma_{\rm el}(0)=4\pi(A^2+C^2)=1434\times10^{-16}$ cm^2.

B. Angle-differential elastic and vibrationally inelastic cross sections

We shall now compare the present calculations with experimental differential elastic and vibrationally inelastic cross sections measured at two representative scattering angles, one in the forward hemisphere (30°) and one in the backward hemisphere (135°). Figure 4 shows the energy loss spectra recorded with a low incident electron energy E_i. Close-lying vibrations, in particular ν_1 and ν_3, are well resolved, like in the 90° high resolution study of Randell *et al.* [48]. The elastic cross section is much larger at the lower scattering angle as expected and as already pointed out by Rohr [16]. The ν_3 peak is also much larger at the smaller scattering angle as expected for a dipole allowed transition and as observed by Rohr [15]. In contrast, the ν_1 and $2\nu_2$ peaks have about the same heights at both scattering angles, indicating an essentially isotropic angular distribution and justifying the *s*-wave assumption of the present theory. Of the remaining vibrations only ν_4 has an appreciable intensity, but substantially weaker than ν_3.

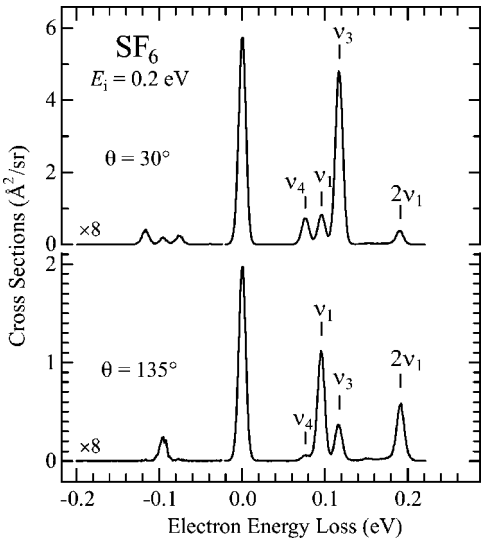

FIG. 4. Electron energy loss spectra recorded with a constant incident energy of 0.2 eV.

In Fig. 5 we present measured differential elastic cross sections and compare them with theory. At energies above 0.1 eV the theory overestimates the cross section at 30° and

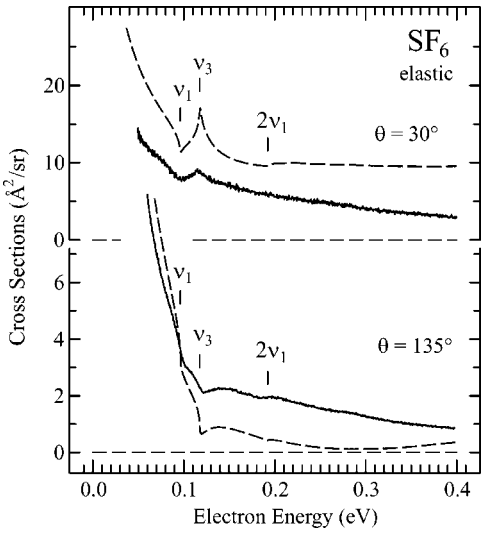

FIG. 5. Theoretical (dashed) and experimental elastic cross sections.

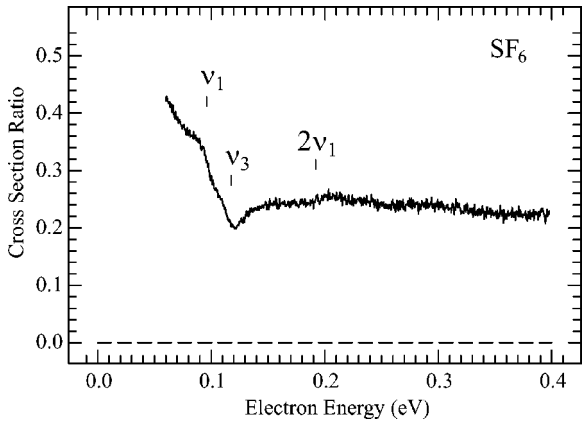

FIG. 6. The ratio $\sigma_{135°}/(\sigma_{30°}+\sigma_{135°})$ of the experimental elastic cross sections.

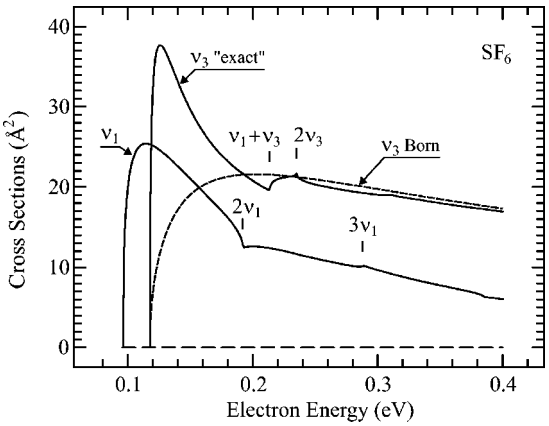

FIG. 7. Calculated integral vibrational excitation cross section.

underestimates it at 135°. We explain this by the inaccuracy of ERT at higher energies, in particular by the neglect of the energy dependence of the logarithmic derivative f. For $\theta = 30°$ the theoretical cross section is too high even at lower energies.

Figure 6 shows the ratio $\sigma_{135°}/(\sigma_{30°}+\sigma_{135°})$ of the experimental elastic cross sections. This ratio becomes 0.5 for isotropic cross section and is, despite the fact that we do not have experimental data integrated over the entire forward and backward hemispheres, a useful measure of the anisotropy because only a slow variation of the cross section with angle is possible at the low energies. The ratio is observed to rise towards 0.5 with decreasing energy, in line with the expected dominance of *s*-wave scattering. It drops with increasing energy because of the forward peaked elastic cross section as already mentioned above. This ratio may be compared qualitatively with the ratio of the backward scattering and the integral scattering cross sections shown in Fig. 6 of Field *et al.* [4], at energies below 100 meV, where vibrational excitation is weak or absent. Both data sets agree that the ratio is around 0.2 at 100 meV, but differ at lower energies. The present ratio starts to rise towards 0.5 immediately below 100 meV, whereas that of Field *et al.* remains at a low value down to an energy of about 20 meV. The degree of anisotroppy in the energy range 20–100 meV observed here is thus less pronounced than that reported by Field *et al.* [4].

Although the ERT theory developed in this paper mainly aims at describing elastic scattering and attachment in the low-energy region below 0.20 eV, it allows us also to calculate vibrational excitation of the ν_1 and ν_3 modes and their overtones. We present here the first theoretical attempt to describe the near-threshold behavior of these processes for SF_6. It should be emphasized, though, that our calculations do not claim high accuracy, but are useful for the investigation of near threshold peaks and cusps.

In Fig. 7 we present vibrational excitation of ν_1 and ν_3 fundamentals. Both cross sections exhibit threshold peaks and cusps at higher VE thresholds. The high transition dipole moment, together with the triple degeneracy of the ν_3 mode, makes the ν_3 cross section very large, even in the Born-dipole approximation. The virtual state effect in the *s*-wave makes the near-threshold cross section even larger leading to a peak value of 37.7×10^{-16} cm^2 at $E=0.126$ eV.

Figure 8 shows the differential cross section for excitation of ν_1. Our theoretical model produces *isotropic* ν_1 cross sections in agreement with the indication from the energy loss spectra in Fig. 4. There is some difference between theory and experiment within 20–30 meV above threshold. The difference is probably of experimental origin—it is very hard to control the collection of 0–30 meV electrons and it seems that the experiment partially suppressed these very slow electrons at 30° and overemphasized them at 135°, possibly because of a weak residual field in the target region. There is a good agreement between theory and experiment at energies above about 130 meV, in particular regarding the structures at vibrational thresholds.

In view of the isotropic behavior, the shape of the present experimental cross section can also be compared with the 90° relative cross section of Randell *et al.* [48]. There is a general agreement in that there is a threshold peak above which the cross section decreases gradually. The peak is

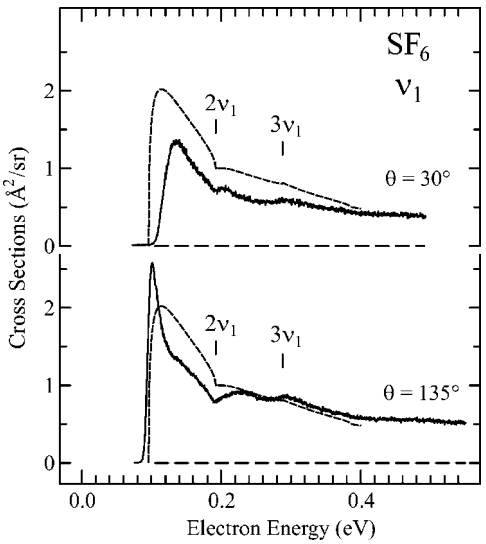

FIG. 8. Theoretical (dashed) and experimental cross sections for excitation of the ν_1 vibration.

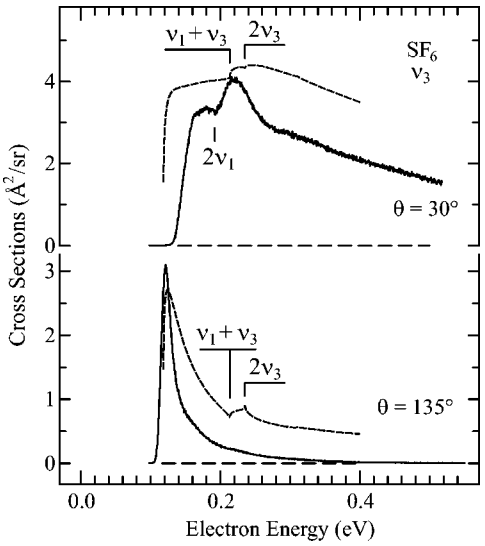

FIG. 9. Theoretical (dashed) and experimental cross sections for excitation of the ν_3 vibration.

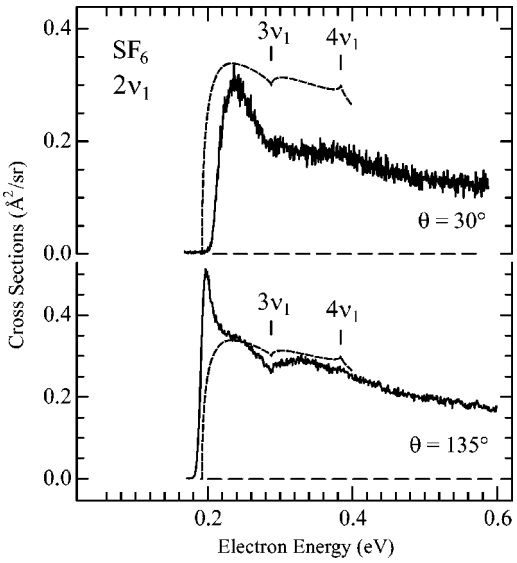

FIG. 10. Theoretical (dashed) and experimental cross sections for excitation of the $2\nu_1$ vibration.

weaker and positioned at higher energy, ~0.2 eV, in the spectrum of Randell *et al.*, however.

In Fig. 9 we present differential cross sections for excitation of the ν_3 mode. In contrast to the ν_1 case, the shape of the theoretical cross section strongly depends on the scattering angle, a finding which agrees qualitatively with that of the measurements. However, the theoretical cross sections are higher. The comparison for $\theta = 135°$ looks particular surprising. One would expect on theoretical grounds that above 0.2 eV the cross section is dominated by the Born-dipole contribution. However, the measured cross section is substantially lower. We should note that at large scattering angles only the first few partial waves (mainly the waves with $l=0$ and $l=1$ in the final state) contribute to the dipole-allowed transition. It might be possible that a non-dipole contribution to these waves cancels the dipole one which would lead to a much smaller cross section than the one obtained in the dipole approximation. Apparently the present calculations do not describe this possible cancellation.

In Fig. 10 we present the cross section for excitation of the first overtone of ν_1. Again, the present experiment appears to suppress electrons below 20 meV at 30° and to overemphasize them at 135°. The calculated cross sections exhibit cusps at higher thresholds due to the virtual-state effect. Structures are seen in the ν_1 cross section at the excitation threshold of $2\nu_1$ and $3\nu_1$, in the ν_3 cross section near the $\nu_1+\nu_3$ and $2\nu_3$ thresholds, and they are especially pronounced in the $2\nu_1$ cross section at the $3\nu_1$ and $4\nu_1$ thresholds.

V. CONCLUSIONS

The present multichannel effective range theory with complex boundary conditions has accounted for the entire complexity of very low energy e-SF_6 scattering, i.e., the elastic and the attachment cross sections, as well as the excitation of the two most important Raman and IR active vibrations. This task is currently far out-of-reach of *ab initio* calculations and has been accomplished here with only two adjustable complex parameters, fitted to the total and the attachment cross sections. This is due to the dominance of *s*-wave scattering in attachment and excitation of the ν_1 vibration. The influence of higher partial waves in elastic scattering and ν_3 excitation was taken into account by incorporation of the proper long-range e-SF_6 interaction. This allowed us also to calculate differential cross sections for elastic scattering and ν_3 excitation. The elastic cross section is found to rise strongly towards low energies. Both theory and experiment confirm the very large magnitudes of the ν_1 and ν_3 vibrationally inelastic cross sections and the presence of threshold peaks. Pronounced narrow structures (cusps) are calculated and observed at vibrational thresholds in all cross sections. Both the present experiment and theory indicate a smaller degree of anisotropy of the elastic cross section in the energy range 0.02–0.1 eV than reported by Field *et al.* [4]. The energy dependent shapes of the phase shifts obtained in the present work differ from those derived by Field *et al.* [4].

ACKNOWLEDGMENTS

The authors thank K. Rohr and J.-P. Ziesel for providing their experimental data in numerical form, and P. D. Burrow, G. A. Gallup, T. M. Miller, T. Hoffmann, M. Braun, and M.-W. Ruf for helpful discussions. I.I.F. has been supported by the US National Science Foundation through Grant No. PHY-0098459 and M.A. by the Swiss National Science Foundation, Project No. 2000-067877.02. H.H. acknowledges support by the Deutsche Forschungsgemeinschaft.

[1] L. G. Christophorou and J. K. Olthoff, J. Phys. Chem. Ref. Data **29**, 267 (2000).
[2] H. Hotop, M.-W. Ruf, M. Allan, and I. I. Fabrikant, Adv. At., Mol., Opt. Phys. **49**, 85 (2003).
[3] J. Ferch, W. Raith, and K. Schröder, J. Phys. B **15**, L175 (1982).
[4] D. Field, N. C. Jones, and J. P. Ziesel, Phys. Rev. A **69**, 052716 (2004).
[5] J. L. Dehmer, J. Siegel, and D. Dill, J. Chem. Phys. **69**, 5205 (1978).
[6] F. A. Gianturco and R. R. Lucchese, J. Chem. Phys. **114**, 3429 (2001).
[7] L. Suess, R. Parthasarathy, and F. B. Dunning, J. Chem. Phys. **117**, 11222 (2002).
[8] E. Vogt and G. H. Wannier, Phys. Rev. **95**, 1190 (1954).
[9] C. E. Klots, Chem. Phys. Lett. **38**, 61 (1976).
[10] J. P. Gauyacq and A. Herzenberg, J. Phys. B **17**, 1155 (1984).
[11] M. Thoss and W. Domcke, J. Chem. Phys. **109**, 6577 (1998).
[12] G. Herzberg, *Infrared and Raman Spectra of Polyatomic Molecules* (Van Nostrand Reinhold, New York, 1945).
[13] T. Uzer, Phys. Rep. **199**, 73 (1991).
[14] G. L. Gutsev and R. J. Bartlett, Mol. Phys. **94**, 121 (1998); R. A. King, J. M. Galbraith, and H. F. Schafer III, J. Phys. Chem. **100**, 6061 (1996); M. Klobukowski, G. H. F. Diercksen, and Garcia de la Vega, Adv. Chem. Phys. **28**, 189 (1997).
[15] K. Rohr, J. Phys. B **10**, 1175 (1977).
[16] K. Rohr, J. Phys. B **12**, L185 (1979); (private communication).
[17] B. I. Schneider, M. LeDourneuf, and P. G. Burke, J. Phys. B **12**, L365 (1979).
[18] I. I. Fabrikant, Comments At. Mol. Phys. **24**, 37 (1990).
[19] I. I. Fabrikant, Phys. Rev. A **43**, 3478 (1991).
[20] D. Klar, M.-W. Ruf, and H. Hotop, Chem. Phys. Lett. **189**, 448 (1992); Aust. J. Phys. **45**, 263 (1992).
[21] J. P. Gauyacq, J. Phys. B **23**, 3041 (1990).
[22] P.-T. Howe, A. Kortyna, M. Darrach, and A. Chutjian, Phys. Rev. A **64**, 042706 (2001).
[23] M. Takekawa and Y. Itikawa, J. Phys. B **32**, 4209 (1999).
[24] T. N. Rescigno, A. E. Orel, A. U. Hazi, and B. V. McKoy, Phys. Rev. A **26**, 690 (1982).
[25] S. B. Hill, M. T. Frey, F. B. Dunning, and I. I. Fabrikant, Phys. Rev. A **53**, 3348 (1996).
[26] I. I. Fabrikant, J. Phys. B **16**, 1253 (1983).
[27] K. Kim, R. S. McDowell, and W. T. King, J. Chem. Phys. **73**, 36 (1980).
[28] D. M. Bishop and L. M. Cheung, J. Phys. Chem. Ref. Data **11**, 119 (1982).
[29] T. M. Miller, in *CRC Handbook of Chemistry and Physics*, 76th ed., edited by D. R. Lide (CRC Press, Boca Raton, FL, 1995), pp. 10, 192–206.
[30] *International Critical Tables* (National Research Council, New York, 1926); G. A. Gallup (private communication).
[31] T. F. O'Malley, L. Rosenberg, and L. Spruch, Phys. Rev. **125**, 1300 (1962).
[32] D. G. Thompson, Proc. R. Soc. London, Ser. A **294**, 160 (1966).
[33] S. V. Hoffmann, S. L. Lunt, N. C. Jones, D. Field, and J.-P. Ziesel, Rev. Sci. Instrum. **73**, 4157 (2002).
[34] H. Hotop, D. Klar, J. Kreil, M.-W. Ruf, A. Schramm, and J. M. Weber, in *The Physics of Electronic and Atomic Collisions*, edited by L. J. Dube, J. B. A. Mitchell, J. W. McConkey, and C. E. Brion, AIP Conf. Proc. No. 360 (AIP Press, Woodbury, NY, 1995), p. 267.
[35] A. Chutjian and S. H. Alajajian, Phys. Rev. A **31**, 2885 (1985).
[36] A. Schramm, J. M. Weber, J. Kreil, D. Klar, M.-W. Ruf, and H. Hotop, Phys. Rev. Lett. **81**, 778 (1998).
[37] S. Barsotti, Dissertation, University of Kaiserslautern, 2002.
[38] D. Klar, M.-W. Ruf, and H. Hotop, Int. J. Mass. Spectrom. **205**, 93 (2001).
[39] Z. Lj. Petrović and R. W. Crompton, J. Phys. B **18**, 2777 (1985).
[40] D. Klar, Dissertation, University of Kaiserslautern, 1993.
[41] M. Allan, J. Phys. B **25**, 1559 (1992).
[42] M. Allan, J. Phys. B **33**, L215 (2000).
[43] A. Gopalan, J Bömmels, S. Götte, A. Landwehr, K. Franz, M.-W. Ruf, H. Hotop, and K. Bartschat, Eur. Phys. J. D **22**, 17 (2003).
[44] R. K. Nesbet, Phys. Rev. A **20**, 58 (1979).
[45] H. Cho, R. J. Gulley, K. W. Trantham, L. J. Uhlmann, C. J. Dedman, and S. J. Buckman, J. Phys. B **33**, 3531 (2000).
[46] I. I. Fabrikant and H. Hotop, Phys. Rev. A **63**, 022706 (2001).
[47] J. P. Ziesel, N. C. Jones, D. Field, and L. B. Madsen, Phys. Rev. Lett. **90**, 083201 (2003).
[48] J. Randell, D. Field, S. L. Lunt, G. Mrotzek, and J. P. Ziesel, J. Phys. B **25**, 2899 (1992).